AGU PUBLICATIONS

JGR

Journal of Geophysical Research: Solid Earth

RESEARCH ARTICLE
10.1002/2016JB013627

Key Points:
- Physics-based constitutive model for lab earthquakes reproduces key observations
- We establish direct connection between the STZ model and rate-and-state friction
- Stick-slip instabilities predicted by STZ model

Correspondence to:
C. K. C. Lieou,
clieou@lanl.gov

Citation:
Lieou, C. K. C., E. G. Daub, R. A. Guyer, R. E. Ecke, C. Marone, and P. A. Johnson (2017), Simulating stick-slip failure in a sheared granular layer using a physics-based constitutive model, *J. Geophys. Res. Solid Earth*, *122*, 295–307, doi:10.1002/2016JB013627.

Received 6 OCT 2016
Accepted 12 JAN 2017
Accepted article online 14 JAN 2017
Published online 28 JAN 2017

Simulating stick-slip failure in a sheared granular layer using a physics-based constitutive model

Charles K. C. Lieou[1,2], Eric G. Daub[3], Robert A. Guyer[1,4], Robert E. Ecke[2,5], Chris Marone[6], and Paul A. Johnson[1,2]

[1]Solid Earth Geophysics Group, Los Alamos National Laboratory, Los Alamos, New Mexico, USA, [2]Center for Nonlinear Studies, Los Alamos National Laboratory, Los Alamos, New Mexico, USA, [3]Center for Earthquake Research and Information, University of Memphis, Memphis, Tennessee, USA, [4]Department of Physics, University of Nevada, Reno, Reno, Nevada, USA, [5]Condensed Matter and Magnetic Science Group, Los Alamos National Laboratory, Los Alamos, New Mexico, USA, [6]Department of Geosciences, Pennsylvania State University, University Park, Pennsylvania, USA

Abstract We model laboratory earthquakes in a biaxial shear apparatus using the Shear-Transformation-Zone (STZ) theory of dense granular flow. The theory is based on the observation that slip events in a granular layer are attributed to grain rearrangement at soft spots called STZs, which can be characterized according to principles of statistical physics. We model lab data on granular shear using STZ theory and document direct connections between the STZ approach and rate-and-state friction. We discuss the stability transition from stable shear to stick-slip failure and show that stick slip is predicted by STZ when the applied shear load exceeds a threshold value that is modulated by elastic stiffness and frictional rheology. We also show that STZ theory mimics fault zone dilation during the stick phase, consistent with lab observations.

1. Introduction

Stick-slip failure is a hallmark of earthquake occurrence and is therefore of fundamental interest to the earthquake physics community. Such behavior has been seen in field studies, in the laboratory, and in numerical simulations [e.g., *Marone*, 1998; *Nasuno et al.*, 1997; *Griffa et al.*, 2011, 2013; *Ferdowsi et al.*, 2014a, 2014b]. Many of these studies suggest that the dynamics of the granular layer, confined under large stresses on the fault, may be crucial in understanding stick-slip instabilities. *Nasuno et al.* [1997] have shown that in a sheared granular material, grain-scale rearrangements occur preceding slip. DEM simulations by *Ferdowsi et al.* [2014a] and *Ferdowsi et al.* [2014b] show that grain movement occurs at the time of, and following, slip. The observation that such local, irreversible rearrangement of grains accounts for plastic deformation and slip in a granular layer is the fundamental idea behind the Shear-Transformation-Zone (STZ) theory of dense granular flow—a physics-based model to describe flow and deformation in discrete particulate media. The theory was originally conceived for, and has been invoked to model, flow in lubricants, bulk metallic glasses, and colloidal materials [e.g., *Falk and Langer*, 1998; *Langer*, 2008; *Daub and Carlson*, 2009; *Falk and Langer*, 2011]. One of the authors of this paper [*Lieou et al.*, 2014a, 2014b, 2015, 2016] extended the range of applicability to granular materials, where the basic units are macroscopic grains as opposed to atoms and molecules. We shall show in this paper how the STZ model behaves in describing velocity-stepping and slide-hold-slide experiments and in describing laboratory earthquakes associated with stick-slip failure. As we shall show, one can make a direct connection between the STZ theory and the rate-and-state constitutive laws. Unlike rate-and-state friction laws which are empirical in character, however, the STZ constitutive model is rooted in grain-scale processes; this provides a pathway for extrapolation across varying length and time scales from the laboratory to the field.

In this paper, we also qualitatively study the effect of the confining stress on the occurrence of stick-slip failure in a sheared granular layer. This focus is motivated by the laboratory observations [e.g., *Anthony and Marone*, 2005], which suggest that stick slip does not occur below a threshold pressure of around 2 MPa in experiments with glass beads in a biaxial shear configuration. (While we use the terminology "stick slip," in the experimental apparatus the material actually "slide slips" due to the near-constant granular motion that accommodates macroscopic shear strain between major slip events.) Dilation is another indication of granular motion

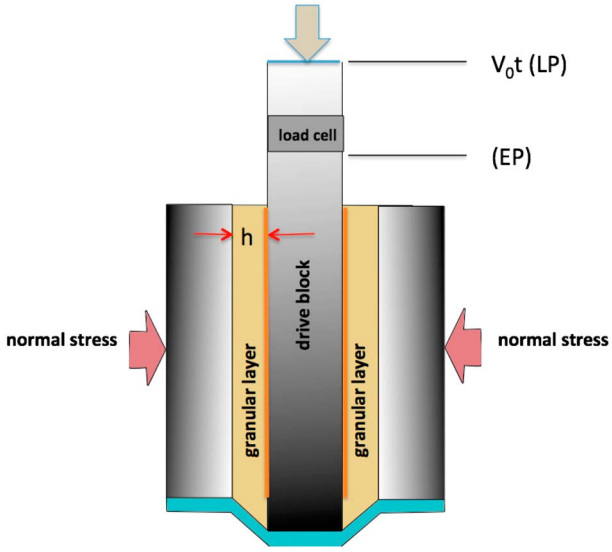

Figure 1. Apparatus of the biaxial experiment. The load cell has an effective stiffness k (see equation (4)); the load point (LP) is displaced at a constant speed v; the displacement of the EP is denoted by x in equation (4). The granular layer is subject to a normal stress p which is held fixed except when going from one stress step to another.

during the "stick" phase between slip events. In the experiments, the granular layer dilates during the "stick" (slide) phase, as the shear stress builds up, and undergoes sudden compaction during slip, as the stress drops abruptly. These experiments also suggest that the stick-slip recurrence time in sheared glass beads decreases with increasing applied load, in contrast, to simulations such as *Aharonov and Sparks* [2004]. We show that with proper selection of a few detailed model ingredients, the STZ theory can qualitatively capture the key features of the biaxial shear experiments. Our results shed light on how one can extrapolate the STZ theory from laboratory experiments to the seismic regime, in order to better understand fault friction and seismic hazards.

2. Experiment

This paper is concerned with experiments performed using the biaxial testing apparatus shown in Figure 1 [e.g., *Marone*, 1998]. Two layers of simulated fault gouge, under constant normal stress, are subjected to shear loading. The normal stress ranges from 2 to 8 MPa. The shear stress and friction on the gouge layers, from the center drive block and measured with a load cell, is an important experimental output. The simulated fault gouge comprises class IV glass spheres (diameter ranging from 105 to 149 μm). The initial layer thickness is 2×4 mm (two layers), and the roughened interfaces with the drive block have dimensions 10 cm × 10 cm. The drive block displacement rate is 5 μm/s. The confining and driving pistons are servo controlled so that constant normal stress and displacement rate of the drive block are maintained at ±0.1 kN and ±0.1 μm/s, respectively. The apparatus is monitored via computer to record load on the drive block and drive block displacement at 10 kHz.

3. Theoretical Model of Shear Transformation Zones

To analyze the experimental observations, we use the Shear-Transformation-Zone (STZ) theory of flow in dense granular media [*Falk and Langer*, 1998, 2011; *Lieou et al.*, 2014a, 2014b, 2015]. The basic idea is that a granular medium deforms and flows, and produces macroscopic friction, only if nonaffine granular rearrangement occurs at weak spots within the material known as STZs. While attempts to construct a theory that tracks the motion of every single grain would be futile, it is in principle possible to describe the motion of STZs statistically using a master equation. This description provides a direct connection between macroscopic friction and the grain-scale physics of deformation; an example of the latter is how grain angularity and surface roughness controls the frictional response of the sheared granular packing [*Lieou et al.*, 2015]. In the past the STZ theory has been applied to physically model constitutive friction laws [*Daub and Carlson*, 2010; *Elbanna and Carlson*, 2014], to explain the formation of a refined gouge layer in conjunction with a theory of

grain fragmentation [*Lieou et al.*, 2014a], to show that stick-slip instabilities arise from intergranular frictional interaction [*Lieou et al.*, 2015], and to suggest how seismic waves cause triggered slow slip [*Lieou et al.*, 2016]. In this section we briefly review the theory; the interested reader is referred to the Appendices and, e.g., *Lieou et al.* [2015, 2016], for details and derivations from basic physical principles.

The number of STZs in each granular assembly is controlled by an effective temperature $\chi \propto \partial V/\partial S_C$, called the compactivity. Quantitatively, an increase in the amount of free volume raises the compactivity and therefore the STZ density Λ according to $\Lambda = 2e^{-1/\chi}$. (See, for example, *Falk and Langer* [2011] and *Lieou et al.* [2014b] for the derivation of this Boltzmann-like relation using the principle of nondecreasing entropy.) In the definition of the compactivity χ, V is the total volume that the granular assembly occupies, and S_C is the entropy of the configurational degrees of freedom (i.e., associated with their relative positions and contacts); the proportionality constant is chosen so that χ is dimensionless. This is analogous to the thermal temperature, except that the energy in its thermodynamic definition is now replaced by the volume.

If one increases the free volume available to a given amount of granular material, there are more ways to pack the grains into the volume V or the thickness h corresponding to a given area, so that the compactivity χ increases with the volume V and, hence, with the layer thickness h. We propose that the relationship between volume and the compactivity is linear in leading approximation. Thus,

$$V = V_0 + \epsilon_1(\chi - \chi_0), \tag{1}$$

where V_0 and χ_0 are constants, and ϵ_1 is the "volume expansion coefficient," analogous to the specific heat in ordinary thermodynamics. A similar expression connects h and χ. Because the evolution of χ is governed by the laws of thermodynamics, its equation of motion can be written down directly once we identify the sources of work and dissipation in the granular medium. The quantity χ is therefore more fundamental than the layer thickness h in controlling the slippage of the granular layer in response to external forcing and is thus the preferred state variable in all subsequent development. In fact, χ is an analog of the thermal temperature; it measures the volume occupied by the fixed number of grains in the same way the thermal temperature measures the energy in a given amount of matter. On the other hand, while χ enters the equations of motion, we can nonetheless use equation (1) to calculate the layer thickness, enabling direct comparison with experiments.

Plastic deformation and flow occurs when grains rearrange irreversibly, changing their relative positions and the local contact network, that is, when STZs "flip" from an orientation that is unstable under the applied stress configuration to a stable one—a so-called "forward" transition. The plastic shear rate $\dot{\gamma}^{\mathrm{pl}}$ is simply the measured slip rate v^{loc} divided by the gouge layer thickness h; it is proportional to the STZ density and the difference between the stress-dependent rate-switching functions and decreases with the fraction of STZs which are stable under the applied stress configuration. Thus,

$$\dot{\gamma}^{\mathrm{pl}} = \frac{4\epsilon_0}{\tau} e^{-1/\chi} R_0 \left[\mathcal{T}(\mu, \chi) - m(\mu, \chi)\right]. \tag{2}$$

In this expression, $\tau = a\sqrt{\varrho_g/p}$ is the time needed for a typical grain of size a and mass density ϱ_g to move by a distance of one grain diameter under the normal load p if it can move at all; the product of this inertial time scale with the shear rate gives the inertial number [*Jop et al.*, 2006]. The macroscopic friction coefficient $\mu = s/p$ is simply the shear-stress-to-pressure ratio. $\mathcal{T}(\mu, \chi) = \tanh(\epsilon_0\mu/\epsilon_Z\chi)$ is the difference between the rate-switching functions $\mathcal{R}(\pm\mu, \chi)$, or the rates for forward and backward STZ transitions, divided by their sum, with ϵ_0 and ϵ_Z being the average STZ core and void volumes in units of the typical grain volume a^3. R_0 is the average of the rate-switching functions; as long as μ is smaller than unity, one can approximate R_0 to be a constant. Meanwhile $m(\mu, \chi)$ represents the difference between the number of STZs of the two orientations divided by their sum; see (A10) in the Appendix for its full expression, which contains an important parameter μ_0. In an unvibrated granular medium, $\dot{\gamma}^{\mathrm{pl}} = 0$ if the stress is small enough such that $\mu\mathcal{T}(\mu, \chi) < \mu_0$, but $m(\mu, \chi) = \mu_0/\mu$ when $\mu\mathcal{T}(\mu, \chi) > \mu_0$. In other words, the parameter μ_0 controls the minimum flow stress without external vibration.

Here as opposed to *Lieou et al.* [2016], we propose that μ_0 is an increasing function of χ. According to *van der Elst et al.* [2012] and *Lieou et al.* [2014b], the present assumption implies that flow instabilities would occur at the shear rates for which the granular layer becomes thinner as a function of increasing imposed shear rate $\dot{\gamma}$ (the interfacial velocity v divided by the shear zone thickness h). Anticipating that the granular layer gets

thinner at small shear rates $\dot{\gamma}$ (see the discussion following equations (9) and (10) below), this means that flow instabilities happen when the shear rate is small enough. We choose the interpolation

$$\mu_0 = \mu_1 + \mu_2 \tanh[B(\chi - \chi_2)], \tag{3}$$

where μ_1, μ_2, B, and χ_2 are constants. While it is *not* a constitutive friction law, this expression gives the minimum dynamic friction in terms of the compactivity χ. It is possible for μ_0 to exhibit other functional dependencies on χ and possibly its rate of change $\dot{\chi}$. For example, one can easily imagine the possibility for the shear resistance to vary with the dilatancy change and therefore $\dot{\chi}$. It is even possible for $\mu_0(\chi)$ to be material dependent. The present assumption, however, makes it possible to fit the key qualitative aspects of experimental observations in a simple manner.

To compute macroscopic friction as a function of the control parameters, one needs to solve the differential equations of motion for μ and χ. The equation for μ, the shear stress divided by the pressure, simply states that the stress increment is directly proportional to the elastic strain increment and can be derived as follows. Assuming that the apparatus has a large, finite stiffness k, the force F in the apparatus is

$$F = k(vt - x) = k_G(x - x^{\mathrm{pl}}). \tag{4}$$

Here v is the loading rate in units of length per unit time, x is the amount of actual slip of the slider, and x^{pl}, being the amount of slip across the entire thickness of the granular material, is proportional to the bulk plastic strain γ^{pl} in the granular layer. The quantity k_G is directly proportional to the aggregate shear modulus G of the granular packing. It follows from some simple algebra that the amount of slip of the slider is

$$x = \frac{vt + rx^{\mathrm{pl}}}{1 + r}, \tag{5}$$

where $r \equiv k_G/k$. As such, upon eliminating the slider displacement x, and dividing through by the pressure p and the shear zone thickness h, the shear stress-to-pressure ratio μ evolves with time as

$$\dot{\mu} = \frac{G/p}{1 + r}(\dot{\gamma} - \dot{\gamma}^{\mathrm{pl}}), \tag{6}$$

where, as before, $\dot{\gamma} = v/h$ represents the imposed shear rate. Note the appearance of the extra prefactor $1/(1 + r)$ compared to the case in which the spring were infinitely stiff. Because the granular layer dilates and becomes less stiff during the stick phase, we assume that G is a function of the compactivity χ:

$$G = \begin{cases} G_0 - G_1\chi; & \text{if } \chi < \chi_4, \\ G_0 - G_1\chi_4; & \text{if } \chi > \chi_4. \end{cases} \tag{7}$$

This functional form of $G(\chi)$ is found to fit the experimental stress measurements reasonably well.

The equation of motion for χ, on the other hand, has the form

$$\epsilon_1\dot{\chi} = \mu\dot{\gamma}^{\mathrm{pl}} - \mathcal{K}(\chi)\chi. \tag{8}$$

Equation (8) is purely a consequence of energy conservation and thermodynamic principles; it simply states that the compactivity increases at a rate proportional to the difference between the rate $\mu\dot{\gamma}^{\mathrm{pl}}$ at which work is done on the granular layer to make it flow and the rate at which energy is dissipated. (If the granular layer is subjected to external vibration, there is an extra term corresponding to the rate at which vibration pumps energy into the system. This term can be neglected if we restrict our analysis to an unvibrated granular layer [*Lieou et al.*, 2016]). The latter is encapsulated in the transport coefficient $\mathcal{K}(\chi)$, which must be nonnegative because of the second law of thermodynamics; it includes dissipation due to inelastic collisions and friction between grains. In the Appendix we derive an expression for $\mathcal{K}$ in terms of the sources of noise—the shearing-induced mechanical noise $\Gamma = \tau\mu\dot{\gamma}^{\mathrm{pl}}/(\epsilon_0\mu_0\Lambda)$ and the noise ξ due to intergranular friction—that set the grains into small-amplitude jiggling motion. As such, equation (8) becomes

$$\dot{\chi} = \frac{2\epsilon_0\mu_0 e^{-1/\chi}}{\tau\epsilon_1}\left[\Gamma\left(1 - \frac{\chi}{\hat{\chi}(q)}\right) - \xi\frac{\chi}{\hat{\chi}(q)}\right] \quad . \tag{9}$$

Here $q \equiv \tau\dot{\gamma}^{\mathrm{pl}}$ is the dimensionless shear rate in the granular layer. In essence, equation (9) simply says that shearing drives the granular layer to the configurational steady state characterized by $\hat{\chi}(q)$, while the intergranular friction ξ dissipates energy and thins the granular layer[*Lieou et al.*, 2015] upon shearing.

As has been discussed in *Lieou et al.* [2015], the frictional interaction between grains, subsumed in ξ, results in the nonmonotonic flow rheology; specifically, the layer thickness and the steady state compactivity χ^{ss}

vary nonmonotonically as functions of the loading rate v. This, together with a χ-dependent μ_0, accounts for rate weakening as well as stick-slip instabilities. Indeed, if $\xi \neq 0$, the compactivity χ can fall below $\hat{\chi}_0$ for a range of slip rates. If χ and therefore the shear zone thickness h decreases with increasing slip rate when the parameter μ_0 rapidly increases with increasing χ, it is possible for the flow stress to decrease as a function of increasing slip rate, thereby accounting for flow instabilities. (The steady state value of χ can be calculated directly by setting $\dot{\chi} = 0$ in equation (9).) A necessary condition for this is that ξ should increase more slowly than the slip rate as the latter increases from 0, while leveling off at fast slip rates, so as to not offset granular layer dilatancy in the latter regime. This has been verified by the shear-cell experiments of *van der Elst et al.* [2012] and our analysis [*Lieou et al.*, 2014b] of their observations.

A straightforward way to produce the desired behavior in both the fast and slow regimes is to specify that

$$\xi = \xi_0 \tanh\left[(\tau_f \dot{\gamma}^{\mathrm{pl}})^2\right]. \tag{10}$$

Here ξ_0 is the upper bound of the noise amplitude that can be caused by friction, and τ_f is a time scale. Contrary to earlier developments [*Lieou et al.*, 2015, 2016], we choose $\xi_0 = p_1/p$ with p_1 being some reference pressure and $\tau_f \propto \sqrt{p}$ – specifically $\tau_f = r_0\sqrt{p}$ where r_0 is a constant. These qualitative dependencies on p imply that increasing the normal load p suppresses the jiggling motion of grains and increases the time of adhesive contact between grains. Other dependencies on p are possible and may depend on the detailed shape and frictional characteristics of the constituent grains. Note that the hyperbolic tangent function is simply an interpolation tool; other functional forms of $\xi(\dot{\gamma}^{\mathrm{pl}})$ that present identical limiting behaviors give rise to the same qualitative features shown in this paper.

The rate-dependent steady state compactivity $\hat{\chi}(q)$, which appears in equation (9), deserves some discussion. It is well documented in the literature [e.g., *van der Elst et al.*, 2012; *Wortel et al.*, 2014] that for smooth grains, layer dilatancy increases with shear rate, but is roughly independent of the shear rate when it is slow enough. Thus, $\hat{\chi}(q)$ is an increasing function of the dimensionless shear rate $q \equiv \tau\dot{\gamma}^{\mathrm{pl}}$, approaching some constant $\hat{\chi}_0$ as $q \to 0$, and increasing without bound as q approaches some critical value. Its full functional form can be found in *Lieou et al.* [2014b] and in Appendix C.

4. Results

Although the STZ approach to fault friction is based entirely on the grain-scale motion in the particulate granular layer and principles of statistical physics, one can draw a direct connection between the STZ model and the rate-and-state constitutive friction laws more familiar to the geophysics community. To this end, we show typical STZ predictions for laboratory velocity-stepping and slide-hold-slide experiments in Figures 2 and 3. Indeed, these results show that our STZ model does predict the typical behavior seen in velocity-stepping and slide-hold-slide experiments [e.g., *Marone*, 1998], often performed to determine properties of the fault gouge material such as the extent of rate weakening and the slip-weakening distance. Specifically, the usual rate-and-state parameters, such as the direct effect A, the evolution effect B, and the slip-weakening distance L, can be related to the STZ model parameters by[*Daub and Carlson*, 2008] as follows:

$$A = p\dot{\gamma}^{\mathrm{pl}} \left.\frac{\partial \mu}{\partial \dot{\gamma}^{\mathrm{pl}}}\right|_{\dot{\gamma}=\dot{\gamma}^{\mathrm{pl}}, \chi=\chi^{\mathrm{ss}}}; \tag{11}$$

$$A - B = p\dot{\gamma}^{\mathrm{pl}} \left.\frac{\partial \mu^{\mathrm{ss}}}{\partial \dot{\gamma}^{\mathrm{pl}}}\right|_{\dot{\gamma}=\dot{\gamma}^{\mathrm{pl}}}; \tag{12}$$

$$L = -\left.\frac{\dot{\gamma}^{\mathrm{pl}}}{\partial \dot{\chi}/\partial \chi}\right|_{\dot{\gamma}=\dot{\gamma}^{\mathrm{pl}}, \chi=\chi^{\mathrm{ss}}}, \tag{13}$$

where μ^{ss} denotes the steady state shear stress-to-pressure ratio. For example, one can directly compute

$$A = \frac{p\left[\tanh\left(\frac{\epsilon_0 \mu^{\mathrm{ss}}}{\epsilon_Z \chi^{\mathrm{ss}}}\right) - \frac{\mu_0}{\mu^{\mathrm{ss}}}\right]}{\frac{\epsilon_0}{\epsilon_Z \chi^{\mathrm{ss}}} \mathrm{sech}^2\left(\frac{\epsilon_0 \mu^{\mathrm{ss}}}{\epsilon_Z \chi^{\mathrm{ss}}}\right) + \frac{\mu_0}{(\mu^{\mathrm{ss}})^2}}. \tag{14}$$

At typical large stresses, this can be approximated as

$$A \approx \frac{p\mu^{\mathrm{ss}}}{\mu_0}(\mu^{\mathrm{ss}} - \mu_0). \tag{15}$$

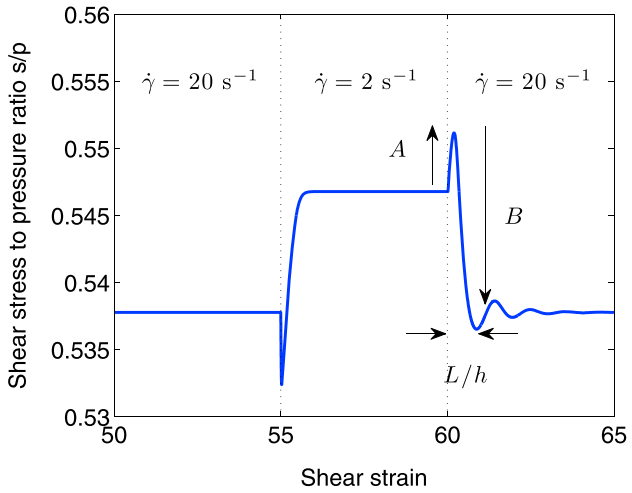

Figure 2. The STZ prediction for the evolution of the shear stress-to-pressure ratio s/p with accumulated shear strain for a typical velocity stepping experiment, outside the regime where stick-slip instabilities occur. The abrupt change of the stress level upon the velocity step, followed by the gradual approach to the steady state, illustrates the connection to rate-and-state friction—the usual rate-and-state parameters A and B, and the slip-weakening distance L divided by the imposed slip rate h, are annotated in the figure. See the end of section 3 for the full expressions of these rate-and-state parameters in terms of STZ state variables.

This suggests that the variation in dynamic friction is small relative to its magnitude. Under the same approximation, one can also calculate

$$A - B \approx p\xi_0 \frac{2\epsilon_0\mu_0 e^{-1/\chi}}{\tau} \frac{\chi}{\hat{\chi}(q) - \chi} \left\{ 2\tau_f^2 \dot{\gamma} \mathrm{sech}^2 \left[(\tau_f \dot{\gamma})^2 \right] - \frac{1}{\dot{\gamma}} \tanh \left[(\tau_f \dot{\gamma})^2 \right] - \frac{\tau}{\hat{\chi}(q) - \chi} \frac{\partial \hat{\chi}}{\partial q} \right\}; \tag{16}$$

$$L \approx \frac{2\epsilon_1 R_0}{\mu_0} \left(1 - \frac{\mu_0}{\mu} \right) \left[\frac{\partial \xi}{\partial \chi} \frac{\chi}{\hat{\chi}(q)} + (\Gamma + \xi) \left(\frac{1}{\hat{\chi}(q)} - \frac{\chi}{(\hat{\chi}(q))^2} \frac{\partial \hat{\chi}}{\partial \chi} \right) \right]^{-1}. \tag{17}$$

The expression for $A - B$ suggests rate-weakening behavior once $\tau_f \dot{\gamma}$ exceeds some threshold. Since we have assumed that $\tau_f \propto \sqrt{p}$, this points to a threshold pressure, for each given shear rate $\dot{\gamma}$, above which the granular layer is rate weakening. On the other hand, the slip-weakening distance L is proportional to ϵ_1 which,

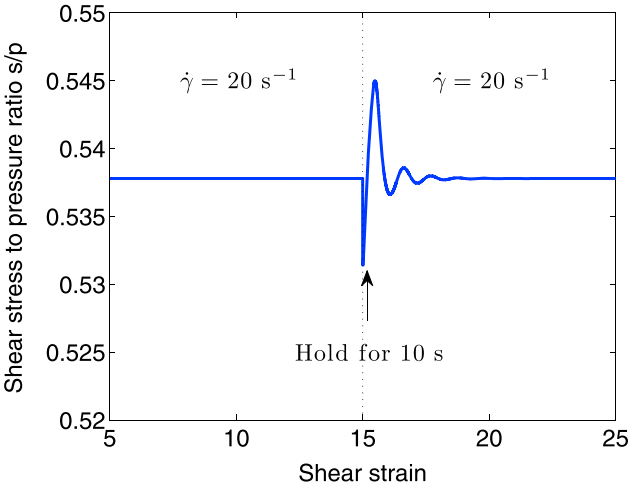

Figure 3. The STZ prediction for the evolution of the shear stress-to-pressure ratio s/p with accumulated shear strain for a typical slide-hold-slide experiment, outside the regime where stick-slip instabilities occur. This is in qualitative agreement with typical observations in sheared granular layers and with model results of rate-and-state friction.

Table 1. List of Parameter Values in the STZ Model Description of Laboratory Faults With Shear Glass Beads and Nature of Parameters (B = Bounded by Experimental Measurements; E = Determined by Experimental Setup; P = Determined by Past Experience and Not Freely Adjusted)

Parameter	Description	Value	Equation	Nature
μ_1	Yield stress parameter	0.35	(3)	B
μ_2	Yield stress parameter	0.2	(3)	B
B	Yield stress parameter	25	(3)	B
χ_2	Yield stress parameter	0.2	(3)	B
a	Grain size	10^{-4} m	τ in (2)	E
ϱ_g	Grain material density	2600 kg/m^3	τ in (2)	E
R_0	Characteristic STZ transition rate	1	(2)	P
p_1	Reference pressure for frictional noise strength ξ_0	2 kPa	(10)	B
r_0	Parameter for frictional time scale τ_f	1.55×10^{-4} s^2 m$^{1/2}$ kg$^{-1/2}$	(10)	P
G_0/p	Aggregate shear modulus parameter	21.6475	(7)	B
G_1/p	Aggregate shear modulus parameter	90	(7)	B
χ_4	Aggregate shear modulus parameter	0.21	(7)	B
$\widehat{\chi}_0$	Steady state compactivity as $q \to 0$	0.3	$\widehat{\chi}(q)$ in (9)	P
ϵ_0	Plastic core volume per STZ in units of grain volume	1.5	(2)	P
ϵ_Z	Excess volume per STZ in units of grain volume	0.5	(2)	P
ϵ_1	Effective volume expansion coefficient	0.3	(9)	P

according to equation (1), is directly proportional to the layer thickness change per unit change in compactivity χ. In other words, the theory suggests that slip-weakening distance is proportional to the variation in layer thickness.

To model stick-slip failure, equations (6) and (9) are numerically integrated with an adaptive time-stepping scheme, for loading rates $v = \dot{\gamma} h = 5\ \mu$m s^{-1}, and normal stresses p between 2 and 8 MPa. The shear zone layer thickness is $h = 500\ \mu$m, so that $\dot{\gamma} = 10^{-2}$ s^{-1}. The initial condition is $\mu(t = 0) = 0.001$ and $\chi(t = 0) = 0.18$. The choice of parameters is summarized in Table 1. Our goal is not to obtain a perfect quantitative agreement with the experimental findings, but to explore the conditions under which the experimental and computational studies find qualitative agreement and ensure that key measures such as the stress drop magnitude, dynamic friction coefficient, recurrence time, and thickness variation are in rough agreement. We will seek quantitative agreement with the experiments described here and elsewhere in future work, possibly through automated parameter search.

Figure 4 shows the temporal evolution of the shear stress, for normal stress p ranging from 2 to 8 MPa. At lower pressures, not shown here for clarity, the granular layer approaches steady sliding. The stick-slip recurrence time of 10–20 s at the shear rate of $\dot{\gamma} = 10^{-2}$ s^{-1} matches that observed in the experiments. We compare

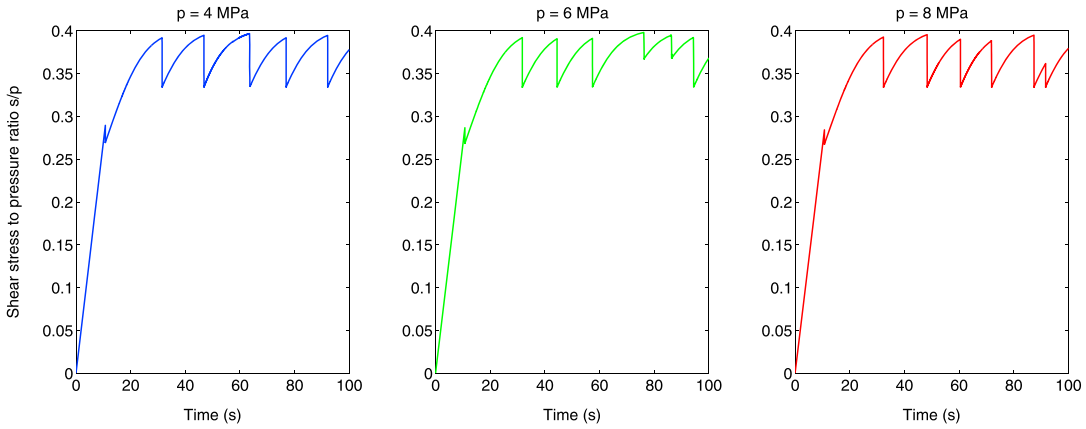

Figure 4. Variation of shear stress to pressure ratio s/p with time t. The pressure ranges from $p = 4$ MPa to 8 MPa. The imposed shear rate is $\dot{\gamma} = 10^{-2}$ s^{-1}. At $p = 2$ MPa and below, not shown here, the sheared granular layer transitions from stick slip to steady sliding.

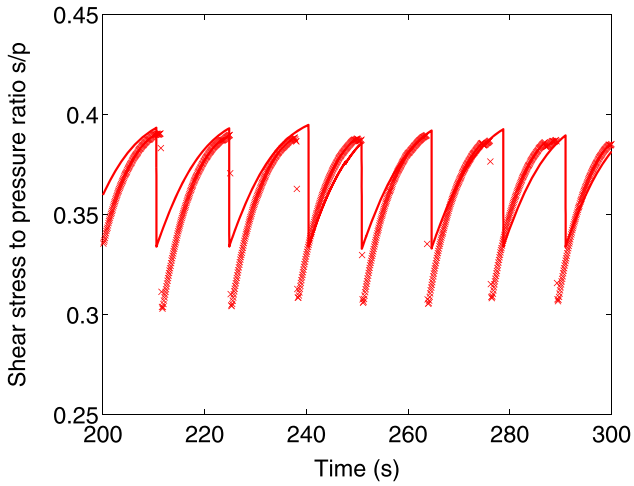

Figure 5. Direct comparison between experiment (crosses) and theory, for the variation of shear stress versus time. For clarity we only show the result for normal stress $p = 8$ MPa; the behavior at lower normal stresses is similar. The imposed shear rate is $\dot{\gamma} = 10^{-2}$ s^{-1} as in above. The experimental data points have been shifted horizontally in time for direct comparison with theory.

the experimental shear stress measurements with the computational results in Figure 5. There is reasonable, albeit imperfect, agreement between the experimental and theoretical results. The fact that we have such agreement with only a handful of adjustable parameters (in addition to some which are determined by the physical setup alone) and simplifying assumptions is rather remarkable. The assumption that the aggregate shear modulus $G(\chi)$ decreases with increasing compactivity χ, or increasing amount of dilation, produces the softening of the granular layer immediately prior to failure. This would not have been possible had we assumed G to be independent of χ—at least not in the parameter space that we have explored.

Figure 6 shows the variation of the compactivity χ and the detrended shear zone layer thickness h (i.e., ignoring the long-time thinning due to the loss of grains) with time. The compactivity χ increases as the shear stress builds up during the stick phase and drops abruptly during slip. This behavior is different from that seen in an earlier version of the STZ model [e.g., *Lieou et al.*, 2015, 2016], but if we assume that the compactivity increases with the thickness of, or extensive volume occupied by, the granular layer according to equation (1), then the present result suggests linear dilation with time of the granular layer during stress buildup, in conformity with experimental observations [e.g., *Marone*, 1998; *Johnson et al.*, 2008]. The connection between the compactivity χ and the thickness h is given by

$$h = h_0 + h_1 \chi \tag{18}$$

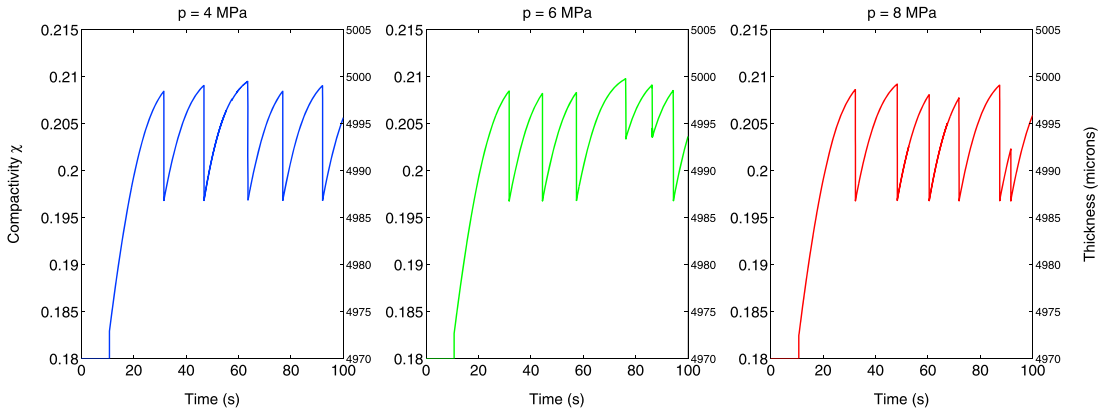

Figure 6. Variation of compactivity χ and shear zone thickness h with time t. The pressures for the blue, green, and red curves are $p = 4$, 6, and 8 MPa, respectively. The imposed shear rate is $\dot{\gamma} = 10^{-2}$ s^{-1}. Notice that the compactivity increases during the stick phase and drops abruptly as slip occurs; the extent of increase is roughly independent of the pressure level. This is in qualitative agreement with the variation of the shear zone thickness with time.

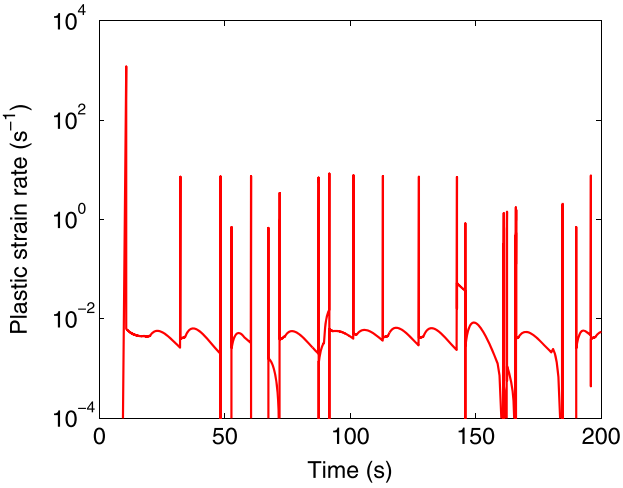

Figure 7. Variation of plastic shear rate $\dot{\gamma}^{pl}$ with time t. The imposed shear rate is $\dot{\gamma} = 10^{-2}$ s^{-1}. For clarity we only show the model results for $p = 8$ MPa; the qualitative features for other pressures are similar. During the stick phase the slip rate does not go to 0; rather, it is roughly an order of magnitude smaller than the imposed slip rate. This is a hallmark of preseismic slip.

with $h_0 = 4.79$ mm and $h_1 = 1$ mm. The drop in thickness during each stress drop is thus roughly 12 μm, in agreement with the experiments.

The fact that the slope of the stress-time curves during the stick phase of repeated stick slip lies below that of the initial loading phase, as seen in Figure 4, suggests that aseismic slip does occur, as in the experiment. This is corroborated by Figure 7, which shows the variation of the plastic shear rate $\dot{\gamma}^{pl}$ with time. Indeed, $\dot{\gamma}^{pl}$ is exceedingly large during slip, as it should be; but it never drops to 0 even during the stick phase. In fact, during stress buildup, $\dot{\gamma}^{pl}$ is almost always less than an order of magnitude smaller than the imposed slip rate of $\dot{\gamma} = 10^{-2}$ s^{-1}.

Finally, we show in Figure 8 a direct comparison of the recurrence interval of slip events predicted by theory and obtained in three sets of glass bead experiments. The agreement with experiments seems to be best for $p = 8$ MPa and remains reasonably good down to $p = 4$ MPa.

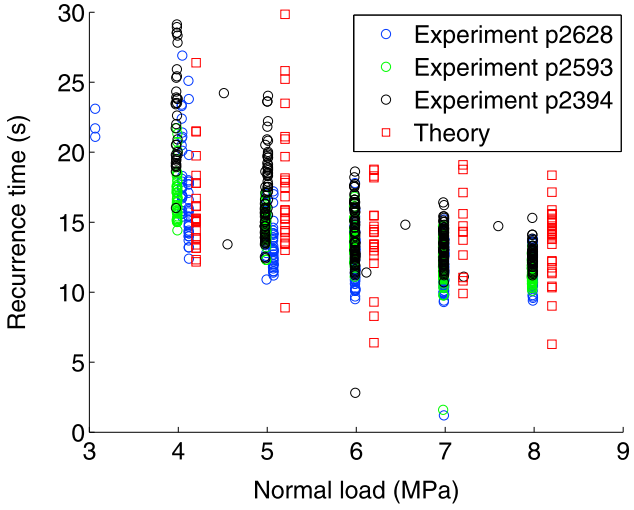

Figure 8. Comparison of the experimental (blue, green, and black circles for the three experimental runs) and theoretical (red squares) recurrence interval of stick-slip events, for normal load p ranging from 4 to 8 MPa. The filled red squares denote the average recurrence time from theory. Note that the red squares have been shifted to the right by 0.2 MPa for clarity.

5. Discussion

In this paper we have refined the STZ theory, a mechanistic model for flow and friction in a sheared granular layer. The STZ model attributes flow and deformation to granular rearrangement at weak spots and quantifies the susceptibility to nonaffine rearrangement through an effective temperature termed the compactivity, which is related to the layer thickness. The laws of nonequilibrium thermodynamics enable us to conveniently deduce the temporal evolution of the stress state and the layer thickness. We have demonstrated the direct connection between the STZ approach and rate-and-state friction, through simulation of velocity-stepping and slide-hold-slide experiments (Figures 2 and 3). In fact, the rate-and-state friction parameters can be deduced from STZ model parameters (equations (11)–(13)); see also *Daub and Carlson* [2008] who drew connections between rate-and-state friction and an earlier version of the STZ theory). The merit of the STZ approach lies in its firm underpinning in statistical physics and the mechanistic origin—granular rearrangement—of slip and deformation in a granular layer. Thus, it becomes possible to trace the origin of the myriad of possible behaviors of sheared fault gouge to the interaction between constituent grains.

Among the key results, we have shown that with a judicious choice of parameters—essentially only a handful of free parameters (others are either fixed by the experimental setup or determined from past experience with sheared granular packings (cf. Table 1))—we have been able to reach reasonably good agreement with results from the biaxial shearing experiment on glass beads. For instance, we have shown that the compactivity increases almost linearly with time during the stick phase and that the extent of the increase is almost independent of the normal load p when it is high enough. This is corroborated by a direct connection between the compactivity and the shear zone thickness (see equation (1)).

The agreement between the experiment and theory in terms of recurrence time of slip events is best for $p = 8$ MPa; we do not attempt to match experimental observations of the dependence of recurrence time with pressure level. Our goal here is to match the general behaviors of slip in glass beads, and we therefore leave such quantitative comparison for future work.

Real earthquakes can involve pressures far above those in laboratory experiments; however, when pore pressures are large, effective pressures may be much reduced, and this could be common in tectonic fault zones. Also, natural fault zones can be much wider than those used in laboratory experiments. Furthermore, properties of the gouge material, such as grain size distribution, mineralogy, and intergranular cohesion, may differ from those of the glass beads in important ways. Despite this, we have demonstrated agreement between our physics-based STZ model and laboratory earthquakes. This suggests that the theory can be scaled to earthquake faults, presumably with different parameter values. We note that acoustic emission recorded on the biaxial shear device is within bounds of the Gutenburg-Richter relation observed at all scales in Earth, indicating that at least some of the frictional physics is captured [*Johnson et al.*, 2013]. This may suggest that the STZ simulation is also capturing some of the pertinent physics. Recent experiments on other materials in place of glass beads, such as the *Leeman et al.* [2016] experiment on quartz powder, suggest that grain geometry and frictional characteristics, which are presently subsumed in the "frictional noise strengh" ξ (equation 10), may play an important role in determining the general behavior. Future efforts will seek to quantitatively identify the material-specific features responsible for the experimentally observed behaviors, through automated determination of system parameters via active learning approaches which we are currently implementing.

Appendix A: Mechanistic Aspects of the STZ Model for Granular Flow

Granular flow and the associated slip occurs because grains rearrange themselves. The sites where grains rearrange are termed shear transformation zones or STZs; these are loose spots in the granular material with excess free volume. An applied shear stress controls whether the grains in a given STZ can move around or whether they are locked in place by the applied stress state. Thus, at a given location within the shear zone, the stress tensor provides a method for classifying STZs, based on the relative orientation of motion. At the macroscale, we can break STZs into two groups; we denote by N_+ and N_- the number of STZs in each of these sets. For cases where the applied stress would cause STZ motion in the "plus" direction, STZs of "minus-type" orientation readily transition (or flip) to become plus type. On the other hand, STZs of plus orientation rarely flip if the applied shear load is large. In these cases, the free volume of an STZ is annihilated by noise, while a new STZ may be created elsewhere. The process of STZ motion, creation, and annihilation is described as

$$\tau \dot{N}_{\pm} = \mathcal{R}(\pm\mu, \chi) N_{\mp} - \mathcal{R}(\mp\mu, \chi) N_{\pm} + \tilde{\Gamma}(N^{eq}/2 - N_{\pm}). \tag{A1}$$

In equation (A1), $\tilde{\Gamma} = \Gamma + \rho$, i.e., the rate of STZ relocation via annihilation and creation is given by the sum of vibrational and shearing terms [*Lieou et al.*, 2016]. The time scale for this process τ is generally chosen as the inertial time scale $\tau = a\sqrt{\varrho_G/p}$, where a, ϱ_G, and p are given by granular properties of size, density, and mean stress. Because intergranular friction does not close or open up voids, the corresponding noise term ξ does not appear in equation (A1).

Let N denote the total number of grains. Then the plastic shear rate is given by the difference between the rate at which plus-type STZs flip and become minus type, and the rate at which the reverse process occurs:

$$\dot{\gamma}^{\mathrm{pl}} = \frac{2\epsilon_0}{\tau N}\left[\mathcal{R}(\mu,\chi)N_- - \mathcal{R}(-\mu,\chi)N_+\right]. \tag{A2}$$

Let us define the intensive variables

$$\Lambda = \frac{N_+ + N_-}{N}; \quad m = \frac{N_+ - N_-}{N_+ + N_-}, \tag{A3}$$

which denote the density and orientational bias of STZs, as well as the symmetric and antisymmetric combinations of the rate-switching function $\mathcal{R}(\pm\mu,\chi)$:

$$\mathcal{C}(\mu,\chi) = \frac{1}{2}\left[\mathcal{R}(\mu,\chi) + \mathcal{R}(-\mu,\chi)\right]; \tag{A4}$$

$$\mathcal{T}(\mu,\chi) = \frac{\mathcal{R}(\mu,\chi) - \mathcal{R}(-\mu,\chi)}{\mathcal{R}(\mu,\chi) + \mathcal{R}(-\mu,\chi)}. \tag{A5}$$

Some straightforward algebra now recasts equation (A2) for the plastic shear rate into

$$\dot{\gamma}^{\mathrm{pl}} = \frac{2\epsilon_0\Lambda}{\tau}\mathcal{C}(\mu,\chi)[\mathcal{T}(\mu,\chi) - m]. \tag{A6}$$

Thus, we arrive at equation (2) in the main text, once we identify $\Lambda = 2e^{-1/\chi}$ for the STZ density from below, and approximate $\mathcal{C}(\mu,\chi) \approx R_0$, where R_0 is a constant of order unity, whenever μ is sufficiently small.

We now rewrite equation (A1) in terms of the order parameters Λ and m as

$$\tau\dot{\Lambda} = \tilde{\Gamma}(\Lambda^{\mathrm{eq}} - \Lambda); \tag{A7}$$

$$\tau\dot{m} = 2\mathcal{C}(\mu,\chi)[\mathcal{T}(\mu,\chi) - m] - \tilde{\Gamma}m - \tau\frac{\dot{\Lambda}}{\Lambda}m. \tag{A8}$$

The diluteness assumption on the STZ population density means that $\Lambda \ll 1$. Because the small factor Λ is absent from the equations for $\dot{\Lambda}$ and $\dot{m}$—which is not the case for (A6) for the plastic shear rate—Λ and m equilibrate much more quickly than the stress and the compactivity. Thus, we can use the stationary values Λ^{eq} and m^{eq}, for which $\dot{\Lambda} = \dot{m} = 0$, in place of Λ and m everywhere henceforth.

Following an argument outlined in, for example, *Lieou et al.* [2015], the second law of thermodynamics yields the stationary STZ density $\Lambda^{\mathrm{eq}} = 2e^{-1/\chi}$ and constrains the rate-switching function to obey $\mathcal{T}(\mu,\chi) = \tanh(\epsilon_0\mu/\epsilon_Z\chi)$. Meanwhile, to compute m^{eq}, recall the proportionality relation between the mechanical noise strength Γ and the energy dissipated per STZ:

$$\Gamma = \frac{\tau\mu\dot{\gamma}^{\mathrm{pl}}}{\epsilon_0\mu_0\Lambda^{\mathrm{eq}}} = \frac{2\mu}{\mu_0}R_0[\mathcal{T}(\mu,\chi) - m], \tag{A9}$$

where μ_0 denotes a stress magnitude. Equation (A9) can be substituted into equation (A7), to yield a stationary case:

$$2R_0[\mathcal{T}(\mu,\chi) - m]\left(1 - \frac{m\mu}{\mu_0}\right) - m\rho = 0, \tag{A10}$$

so that

$$m^{\mathrm{eq}} = \frac{\mu_0}{2\mu}\left[1 + \frac{\mu}{\mu_0}\mathcal{T}(\mu,\chi) + \frac{\rho}{2R_0}\right] - \frac{\mu_0}{2\mu}\sqrt{\left[1 + \frac{\mu}{\mu_0}\mathcal{T}(\mu,\chi) + \frac{\rho}{2R_0}\right] - \frac{4\mu}{\mu_0}\mathcal{T}(\mu,\chi)}.$$

In particular, when $\rho = 0$—that is, if there is no external vibration—this gives

$$m^{\text{eq}} = \begin{cases} \mathcal{T}(\mu, \chi), & \text{if } (\mu/\mu_0)\mathcal{T}(\mu, \chi) < 1; \\ \mu_0/\mu, & \text{if } (\mu/\mu_0)\mathcal{T}(\mu, \chi) \geq 1. \end{cases} \tag{A11}$$

It becomes transparent that the proportionality parameter μ_0 between the plastic work rate and the intensity Γ of mechanical noise sets the minimum flow stress of an unvibrated granular layer. Otherwise, if there is external vibration, $\rho \neq 0$ and flow can occur at stresses far below μ_0.

Appendix B: Derivation of Equation (9) From (8)

The key to deriving equation (9) for the evolution of χ from equation (8) primarily involves computing the transport coefficient $\mathcal{K}$ that describes energy dissipation in the sheared granular layer. In the absence of external vibrations, $\mathcal{K}$ is controlled by shearing and intergranular friction. The first step of the derivation is to determine $\mathcal{K}$ for smooth frictionless grains; the effect of frictional granular contacts will be exploited afterwards.

For frictionless grains the steady state compactivity $\hat{\chi}(q)$ is determined solely by the dimensionless form of the shear rate $q \equiv \tau\dot{\gamma}^{\text{pl}}$. Putting $\dot{\chi} = 0$ and $\chi = \hat{\chi}(q)$ into equation (8) gives

$$\mathcal{K} = \frac{W}{\hat{\chi}(q)}, \tag{B1}$$

where $W = \tau\mu\dot{\gamma}^{\text{pl}}$ is a dimensionless plastic work rate.

Frictional contact between grains provides another means of dissipation, with corresponding (dimensionless) dissipation rate F. As such, we postulate that the above expression for $\mathcal{K}$ can be modified as

$$\mathcal{K}(\chi) = \frac{1}{\tau}\frac{W + F}{\hat{\chi}(q)}. \tag{B2}$$

Hence, equation (8) for the evolution of χ becomes

$$\epsilon_1\dot{\chi} = \frac{W}{\tau} - \frac{W + F}{\tau}\frac{\chi}{\hat{\chi}(q)}. \tag{B3}$$

It remains to relate the dissipation rates W and F to the corresponding noise strengths. As in the discussion leading to equation (A9), the strength Γ of mechanical noise is proportional to the rate of energy dissipation per STZ [*Lieou et al.*, 2015]. Thus,

$$W = \Gamma\epsilon_0\mu_0\Lambda. \tag{B4}$$

The dimensionless number μ_0 was introduced in the main text as a parameter that controls the flow stress; equation (B4) is the origin of this parameter. Next, we postulate that the frictional dissipation be proportional to the number of weak spots undergoing rearrangement and therefore the population of STZs. Hence, the frictional noise strength ξ and the corresponding dissipation rate F are related through

$$F = \xi\epsilon_0\mu_0\Lambda. \tag{B5}$$

Equation (9) follows immediately from the substitution of equations (B4) and (B5) into (8).

Appendix C: Rate-Dependent Steady State Compactivity $\hat{\chi}(q)$

When an unvibrated collection of frictionless grains is strained at a dimensionless shear rate q, it must approach a steady state with corresponding compactivity $\hat{\chi}(q)$ introduced in section 3. As has been foreshadowed in the main text, $\hat{\chi}(q)$ quantifies rate-dependent dilatancy; it approaches some nonzero constant $\hat{\chi}_0$ as the strain rate goes to 0 and diverges as q approaches some critical strain rate q_0. Motivated by the Vogel-Fulcher function that appears in the viscosity of a strained amorphous solid, we use the following functional form to interpolate between the two limits[*Lieou et al.*, 2015]

$$q(\hat{\chi}) = q_0 \exp\left[-\frac{A}{\hat{\chi}} - \alpha_{\text{eff}}(\hat{\chi})\right], \tag{C1}$$

where

$$\alpha_{\text{eff}}(\hat{\chi}) = \left(\frac{\hat{\chi}_1}{\hat{\chi} - \hat{\chi}_0}\right) \exp\left(-3\frac{\hat{\chi} - \hat{\chi}_0}{\hat{\chi}_A - \hat{\chi}_0}\right). \tag{C2}$$

The parameter values used in this paper are $\hat{\chi}_0 = 0.3$, $\hat{\chi}_1 = 0.02$, $\hat{\chi}_A = 0.33$, $A = 2$, and $q_0 = 2$; these are identical to those used in *Lieou et al.* [2014b], *Lieou et al.* [2015], and *Lieou et al.* [2016].

Acknowledgments
We gratefully acknowledge the support of the US DOE Office of Science, Geosciences Division. C.L. was also partially supported by the Center for Nonlinear Studies at the Los Alamos National Laboratory, with funds from Institutional Support (LDRD). The LANL release number of this article is LA-UR-16-26676. The data used in this paper can be obtained by contacting the corresponding author.

References

Aharonov, E., and D. Sparks (2004), Stick-slip motion in simulated granular layers, *J. Geophys. Res.*, *109*, B09306, doi:10.1029/2003JB002597.
Anthony, J. L., and C. Marone (2005), Influence of particle characteristics on granular friction, *J. Geophys. Res.*, *110*, B08409, doi:10.1029/2004JB003399.
Daub, E. G., and J. M. Carlson (2008), A constitutive model for fault gouge deformation in dynamic rupture simulations, *J. Geophys. Res.*, *113*, doi:10.1029/2007JB005377.
Daub, E. G., and J. M. Carlson (2009), Stick-slip instabilities and shear strain localization in amorphous materials, *Phys. Rev. E*, *80*, 66113, doi:10.1103/PhysRevE.80.066113.
Daub, E. G., and J. M. Carlson (2010), Friction, fracture, and earthquakes, *Annu. Rev. Conden. Matter Phys.*, *1*(1), 397–418, doi:10.1146/annurev-conmatphys-070909-104025.
Elbanna, A. E., and J. M. Carlson (2014), A two-scale model for sheared fault gouge: Competition between macroscopic disorder and local viscoplasticity, *J. Geophys. Res. Solid Earth*, *119*, 4841–4859, doi:10.1002/2014JB011001.
Falk, M. L., and J. Langer (2011), Deformation and failure of amorphous, solidlike materials, *Annu. Rev. Conden. Matter Phys.*, *2*(1), 353–373, doi:10.1146/annurev-conmatphys-062910-140452.
Falk, M. L., and J. S. Langer (1998), Dynamics of viscoplastic deformation in amorphous solids, *Phys. Rev. E*, *57*, 7192–7205, doi:10.1103/PhysRevE.57.7192.
Ferdowsi, B., M. Griffa, R. A. Guyer, P. A. Johnson, C. Marone, and J. Carmeliet (2014a), Three-dimensional discrete element modeling of triggered slip in sheared granular media, *Phys. Rev. E*, *89*, 42204, doi:10.1103/PhysRevE.89.042204.
Ferdowsi, B., M. Griffa, R. Guyer, P. Johnson, and J. Carmeliet (2014b), Effect of boundary vibration on the frictional behavior of a dense sheared granular layer, *Acta Mech.*, *225*(8), 2227–2237, doi:10.1007/s00707-014-1136-y.
Griffa, M., E. G. Daub, R. A. Guyer, P. A. Johnson, C. Marone, and J. Carmeliet (2011), Vibration-induced slip in sheared granular layers and the micromechanics of dynamic earthquake triggering, *Eur. Lett.*, *96*(1), 14001.
Griffa, M., B. Ferdowsi, R. A. Guyer, E. G. Daub, P. A. Johnson, C. Marone, and J. Carmeliet (2013), Influence of vibration amplitude on dynamic triggering of slip in sheared granular layers, *Phys. Rev. E*, *87*, 12205, doi:10.1103/PhysRevE.87.012205.
Johnson, P. A., H. Savage, M. Knuth, J. Gomberg, and C. Marone (2008), Effects of acoustic waves on stick slip in granular media and implications for earthquakes, *Nature*, *451*, 57–60.
Johnson, P. A., B. Ferdowsi, B. M. Kaproth, M. Scuderi, M. Griffa, J. Carmeliet, R. A. Guyer, P.-Y. Le Bas, D. T. Trugman, and C. Marone (2013), Acoustic emission and microslip precursors to stick-slip failure in sheared granular material, *Geophys. Res. Lett.*, *40*(21), 5627–5631, doi:10.1002/2013GL057848.
Jop, P., Y. Forterre, and O. Pouliquen (2006), A constitutive law for dense granular flows, *Nature*, *447*, 727–730.
Langer, J. S. (2008), Shear-transformation-zone theory of plastic deformation near the glass transition, *Phys. Rev. E*, *77*, 21502, doi:10.1103/PhysRevE.77.021502.
Leeman, J. R., D. M. Saffer, M. M. Scuderi, and C. Marone (2016), Laboratory observations of slow earthquakes and the spectrum of tectonic fault slip modes, *Nat. Commun.*, *7*, 11104, doi:10.1038/ncomms11104.
Lieou, C. K. C., A. E. Elbanna, and J. M. Carlson (2014a), Grain fragmentation in sheared granular flow: Weakening effects, energy dissipation, and strain localization, *Phys. Rev. E*, *89*, 22203, doi:10.1103/PhysRevE.89.022203.
Lieou, C. K. C., A. E. Elbanna, J. S. Langer, and J. M. Carlson (2014b), Shear flow of angular grains: Acoustic effects and nonmonotonic rate dependence of volume, *Phys. Rev. E*, *90*, 32204, doi:10.1103/PhysRevE.90.032204.
Lieou, C. K. C., A. E. Elbanna, J. S. Langer, and J. M. Carlson (2015), Stick-slip instabilities in sheared granular flow: The role of friction and acoustic vibrations, *Phys. Rev. E*, *92*, 22209, doi:10.1103/PhysRevE.92.022209.
Lieou, C. K. C., A. E. Elbanna, and J. M. Carlson (2016), Dynamic friction in sheared fault gouge: Implications of acoustic vibration on triggering and slow slip, *J. Geophys. Res. Solid Earth*, *121*, 1483–1496, doi:10.1002/2015JB012741.
Marone, C. (1998), Laboratory-derived friction laws and their application to seismic faulting, *Annu. Rev. Earth Planet. Sci.*, *26*(1), 643–696, doi:10.1146/annurev.earth.26.1.643.
Nasuno, S., A. Kudrolli, and J. P. Gollub (1997), Friction in granular layers: Hysteresis and precursors, *Phys. Rev. Lett.*, *79*, 949–952, doi:10.1103/PhysRevLett.79.949.
van der Elst, N. J., E. E. Brodsky, P.-Y. Le Bas, and P. A. Johnson (2012), Auto-acoustic compaction in steady shear flows: Experimental evidence for suppression of shear dilatancy by internal acoustic vibration, *J. Geophys. Res.*, *117*, B09314, doi:10.1029/2011JB008897.
Wortel, G. H., J. A. Dijksman, and M. van Hecke (2014), Rheology of weakly vibrated granular media, *Phys. Rev. E*, *89*, 12202, doi:10.1103/PhysRevE.89.012202.